Is There a Magnetic Field Effect on Electrochemical Kinetics?

Olivier Devos,* Omar Aaboubi, Jean-Paul Chopart, and Alain Olivier

CNRS, EP 120 "Dynamique des Transferts aux Interfaces", UFR Sciences, BP 1039, 51687 Reims Cedex 02, France

Claude Gabrielli and Bernard Tribollet

CNRS, UPR 15, "Physique des Liquides et Électrochimie", Université Pierre et Marie Curie, Tour 22, 4 Place Jussieu, 75252 Paris Cedex 05, France

Received: October 18, 1999

Whether the influence of magnetic field **B** on the diffusion process during an electrochemical reaction is now well known, the magnetic field effects on the electrochemical kinetics are still a subject of controversy. We have investigated, by means of electrochemical impedance spectroscopy, different electrochemical systems, mass transport controlled, kinetically controlled, and mixed systems, under superimposed **B**. All results led to the conclusion that a homogeneous **B** parallel to the electrode surface and varying up to 1 T had no effect on the charge-transfer coefficient.

Introduction

It is well known that an electrolytic current controlled by a mass transport process is modified when a homogeneous magnetic field is applied parallel to the electrode surface (see refs 1 and 2 and references therein and refs 3 and 4). It was shown that, in the case of a redox process, the stationary limiting diffusion current on a steady electrode is proportional to $\mathbf{B}^{1/3}C^{*4/3}$, where **B** is the magnetic field and C^* is the electroactive species concentration.[5−7] It was established that this phenomenon is due to a unidirectional magnetohydrodynamic (MHD) flow induced by **B** along the electrochemical interface.[8] Some recent investigations have also proposed to introduce the existence of another magnetic force generated in the presence of a nonuniform **B**.[9,10] This latter force involved a motion of the electrolytic solution depending on its magnetic properties,[11,12] but it is more efficient when the magnetic field is perpendicular to the electrode surface. On the other hand, during the electrochemical reaction, the influence of **B** on the charge-transfer rate is still a subject of controversy. In the case of copper electrodeposition, it was shown that **B** does not modify the exchange current and the charge-transfer kinetic at the electrode/solution interface.[13,14] Nevertheless, other authors have shown an apparent shift of the charge-transfer coefficient with **B**.[15−17]

In this study we proposed to investigate different electrochemical systems under superimposed **B**. The charge-transfer rate was analyzed by means of electrochemical impedance spectroscopy (EIS). Indeed, the high-frequency range of the experimental diagrams led to obtainment of the cathodic or anodic charge-transfer coefficient for different **B** intensities. By using this transient method, we have chosen to investigate three types of systems, fast redox systems, mixed redox systems, and kinetically controlled systems. To extract the magnetic field effect on the kinetically controlled processes, a so-called "nonconvective" electrode was also used to prevent the convection generated by the MHD effect. The experimental data were compared with the data obtained by using a classical convective cell.

Experimental Section

A classical three-electrode cell was used to carry out the experiments. The three electrodes were connected to a potentiostat (Solartron 1286). For the impedance measurements, the frequency response analyzer was a Solartron 1253. The electrolyte was kept at room temperature by circulating a thermostatic control water in a double-jacketed cell. The cell was settled in the gap of an electromagnet (Drush EAM 20G). The pole pieces 20 cm in diameter were large enough to apply a homogeneous magnetic field up to 1 T on the whole experimental device. **B** was parallel to the surface of the working electrode. The $\mathbf{B} = 0$ experiments were performed outside the electromagnet to prevent any remanent magnetic field. The nonconvective electrode was built by inserting the working electrode in a hole, which had the same diameter as the electrode, drilled in an insulator (Figure 1). This type of protected electrode has already been used for chronopotentiometric investigations by A. J. Bard[18] and H. B. Mark[19] to maintain some linear diffusion conditions and to reduce the effects of the natural convection.

Theory

Owing to an electrochemical reaction such as

$$\mathrm{Ox} + n\,\mathrm{e}^- \rightleftarrows \mathrm{Red}$$

where n is the number of electrons involved in the reaction, the electrolytic current is written as follows:

$$I = nFAk_aC_{\mathrm{Red}}(0,t) - nFAk_cC_{\mathrm{Ox}}(0,t) \qquad (1)$$

where F is the Faraday constant, A is the electrode surface, k_a and k_c are the anodic and cathodic kinetic constants, and

* To whom correspondence should be addressed. E-mail: o_devos@yahoo.com. Fax: 33.3.23.38.00.39.

10.1021/jp993696v CCC: $19.00
Published on Web 02/01/2000

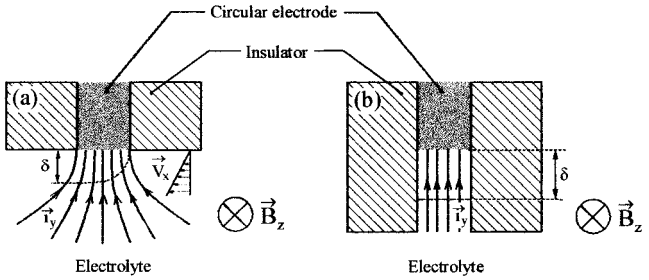

Figure 1. Side view of the convective electrode[6] (a) and the nonconvective electrode (b). **B** = magnetic field, i = electrolytic current, υ = fluid velocity induced by **B**, and δ = thickness of the diffusion layer.

$C_{Red}(0,t)$ and $C_{Ox}(0,t)$ are the surface concentrations of species Red and Ox on the electrode.

For high polarization, one of the terms in eq 1 is negligible

$$I = \pm nFAkC_i(0,t) \qquad \text{i} = \text{Ox or Red} \tag{2}$$

where

$$k = k_0 e^{bV} \tag{3}$$

$$b = -\frac{\alpha nF}{RT} \qquad \text{for a cathodic process} \tag{4}$$

and

$$b = \frac{\beta nF}{RT} \qquad \text{for an anodic process} \tag{5}$$

k_0 is the intrinsic kinetic constant, V is the applied potential, α and β are the cathodic and anodic charge-transfer coefficients, R is the gas constant, and T is the temperature.

Thus, for the kinetically controlled reaction, the response of the faradaic current to a small-amplitude potential perturbation is related by

$$\left(\frac{\partial I}{\partial V}\right)_{C_i} = \frac{1}{R_{ct}} = Ib \tag{6}$$

where R_{ct} is the charge-transfer resistance. Therefore

$$R_{ct}I = b^{-1} \tag{7}$$

The $R_{ct}I$ value leads to characterization of the charge-transfer coefficient of the electrochemical reaction. The R_{ct} value is obtained by means of EIS investigation for different **B** intensities as the intersection of the low-frequency extrapolation of the high-frequency loop.

Results and Discussion

1. Mass Transport Controlled System: $K_3Fe(CN)_6/K_4Fe(CN)_6$. *1.1. Current−Voltage Curves.* Figure 2a shows the current−voltage curves obtained with a convective electrode for different **B** intensities. The platinum working electrode was positioned vertically. The counter electrode was a large platinum sheet, and the reference electrode was a saturated calomel electrode (SCE). According to the previous works,[7,20] the MHD convection generated along the electrode surface enhanced the cathodic and anodic limiting current values. On the contrary, by using the nonconvective electrode, no increase of the limiting current was noticed in the presence of **B**, and rather a tendency to a slight decrease was observed, especially on the cathodic side (Figure 2b). This phenomenon was assumed to be a residual

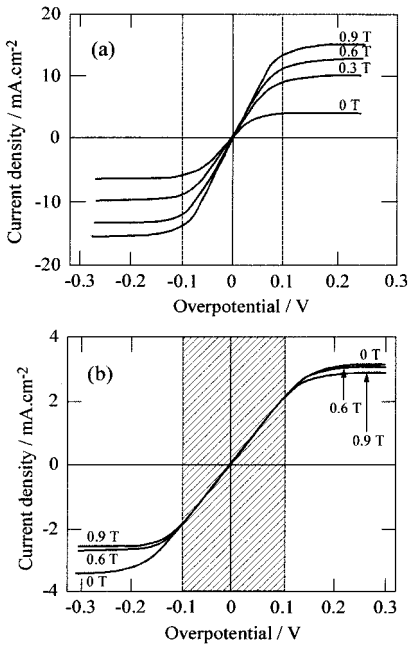

Figure 2. Current density−voltage curves for various **B** intensities: (a) convective electrode, electrode diameter 2 mm, (b) nonconvective electrode, electrode diameter 5 mm. Ferricyanide/ferrocyanide redox system. $[Fe(CN)_6^{3-}] = [Fe(CN)_6^{4-}] = 0.1$ M, [KCl] = 1 M.

effect of the MHD and natural convection. In addition, without magnetic induction, the current density was clearly lower than in the case of the convective electrode. This decrease could be likely attributed to the fact that the diffusion process is only in the direction perpendicular to the nonconvective electrode. With the usual electrode, the diffusion is more spherical, which increases the flux at the electrode edge. Thus, in the overpotential domain corresponding to the dashed area in Figure 2b, the nonconvective electrode could be readily used to prevent the forced convection generated by **B** and to extract any change of the interfacial kinetic process by using EIS investigation.

1.2. EIS Investigation. In the case of the convective electrode, the impedance diagrams are represented in Figure 3a in the Nyquist plane for various **B** intensities and cathodic polarization. The observed loops characterized the diffusion process of the $Fe(CN)_6^{3-}$ ions toward the electrode. The magnitude of the diffusion loop decreased with **B** in agreement with previous works using a supporting electrolyte.[6,7,20] The MHD convection induced an increase of the electrolytic current, which led to a decrease of the diffusion layer thickness. The same evolution of the diagrams was also obtained by means of a classical forced convection tool, namely, the rotating disk electrode. The diagrams obtained from the nonconvective electrode are presented in Figure 3b. In this case, the high-frequency semicircle which characterized the double-layer capacity, C_d, in parallel with the charge-transfer resistance, R_{ct}, was clearly separated from the diffusion loop in the low-frequency range. Indeed, as the forced convection was eliminated and the free convection was diminished, the characteristic frequency of the mass transport was much lower, which led to a thicker diffusion layer. A superimposition of **B** did not change the high- and low-frequency loops. According to the previous study in the steady state, a magnetic field applied on a nonconvective electrode has no influence on the diffusion process due to the absence of the MHD convective flux. Moreover, for a rapid redox system such as $Fe(CN)_6^{3-}/Fe(CN)_6^{4-}$, it was not possible to distinguish any effect of **B** on the charge-transfer process as the charge-transfer resistance did not change.

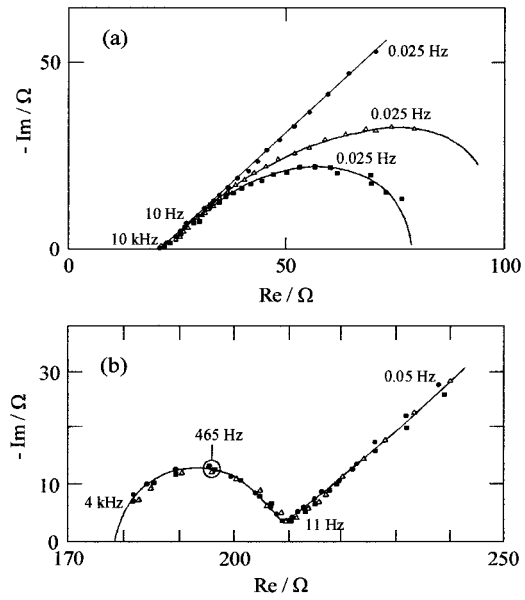

Figure 3. Electrochemical impedances in the Nyquist plane for various **B** intensities: (a) convective cell, electrode diameter 2 mm, (b) nonconvective cell, electrode diameter 5 mm; (●) **B** = 0, (△) **B** = 0.3 T, (■) **B** = 0.6 T. Ferricyanide/ferrocyanide redox system. $[Fe(CN)_6^{3-}] = [Fe(CN)_6^{4-}] = 0.075$ M, overpotential −70 mV.

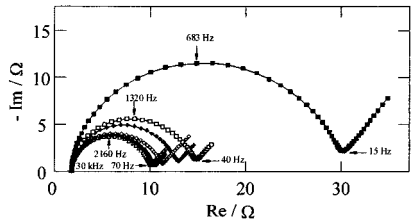

Figure 4. Electrochemical impedances in the Nyquist plane for various **B** intensities: (■) **B** = 0, (□) **B** = 0.15 T, (◆) **B** = 0.3 T, (◇) **B** = 0.45 T, (▲) **B** = 0.75 T, (△) **B** = 0.9 T. $Zn(OH)_4^{2-}$/Zn system with the convective electrode. $[Zn(OH)_4^{2-}] = 0.15$ M, [KOH] = 7 M, overpotential −75 mV, electrode diameter 5 mm.

2. Mixed Redox Systems. *2.1. Zinc Electrodeposition from a Basic Medium.* The $Zn(OH)_4^{2-}$/Zn system is known to be both mass transport and kinetically controlled. The influence of **B** on the diffusion process during zinc electrodeposition from a basic medium was already studied in a previous work.[21] The EIS investigation had highlighted the existence of two diffusing species, zincate and hydroxyle ions, involved in the mechanism. The good agreement between the experimental diffusion loops and the fitted curves provided some kinetic parameters of the reaction process. These coefficients were not modified in the presence of **B** for a convective electrode. In this study, the high-frequency domain of the impedance diagrams, which was directly related to the charge-transfer kinetic process, was analyzed. The working electrode was a circular zinc disk facing downward. The counter electrode was a large-surface zinc-soluble anode, and the reference electrode was a Hg/HgO/KOH (5 M) electrode. The electrolytic solution was prepared by dissolving ZnO and KOH in permuted water. The impedance diagrams are represented in Figure 4 for an overpotential corresponding to 3/4 of the limiting current value. In comparison with a fast redox system, the high-frequency loop obtained for a mixed system was readily isolated by using a classical convective electrode. The magnitude of the high-frequency impedance strongly decreased with superimposition of **B**. Respectively, an increase of the electrolytic current I due to the forced convection generated in the vicinity of the electrode surface was measured. A calculated curve was adjusted on the experimental semicircles from a fitting program by using the following classical equation of the impedance Z:

$$Z = R_s + \frac{R_{ct}}{1 + jC_dR_{ct}\omega} \tag{8}$$

where R_s is the solution resistance, ω is the pulsation, and $j = \sqrt{-1}$.

The good agreement between the fitted curve and the experimental curve led to good accuracy in the R_{ct}, C_d, and R_s values. The R_{ct}, C_d, and I values and the product $R_{ct}I$ are shown in Table 1 for different **B** intensities. It is noticeable that the C_d values were not affected by **B**. Moreover, the product $R_{ct}I$ was practically constant in the present experimental conditions when **B** was changed. Thus, for a convective electrode, the magnetic field did not affect the product $R_{ct}I$, which corresponds to the charge-transfer coefficient as demonstrated previously, eq 7. This result confirmed a previous study performed with another mixed system, the copper electrodeposition from an acidic medium.[13]

To complete this section, two other mixed systems, $FeCl_3$/$FeCl_2$ and copper electrodissolution, were analyzed. In both cases, the EIS investigation was performed when the electrode was polarized at low overpotential to reduce the contribution of the diffusion process in the mechanism.

2.2. $FeCl_3$/$FeCl_2$ in 4 M HCl. The platinum working electrode was vertically positioned. The counter electrode was a platinum grid, and a SCE reference electrode was used. The impedance diagrams corresponding to a low cathodic overpotential are represented in Figure 5a for the convective electrode and Figure 5b for the nonconvective electrode. In both cases, the presence of a Warburg straight line inclined at 45° on the real axis, which is characteristic of the diffusion process, was observed. For the convective electrode, the experimental current values I as well as the high-frequency loops (Figure 5a) did not practically change when a superimposed **B** was changed. The fitted curves obtained from eq 8 led to the mean values of $C_d = 100\ \mu F \cdot cm^{-2}$ and $R_{ct} = 2.2\ \Omega \cdot cm^2$ for **B** intensities up to 1 T. Thus, for low overpotentials, the magnetic field had no effect on the electrolytic current, which was kinetically controlled. This result was confirmed by using the nonconvective electrode. The following constant values were obtained for different **B** intensities: $C_d = 100\ \mu F \cdot cm^{-2}$ and $R_{ct} = 7.9\ \Omega \cdot cm^2$.

2.3. Copper Electrodissolution. The working electrode was a copper disk facing upward. The counter electrode was a large surface platinum electrode, and the reference electrode was a saturated sulfate electrode (SSE). The electrolytic solution was prepared by dissolving $CuSO_4 \cdot 5H_2O$ in H_2SO_4 (0.5 M). The impedance diagrams are shown in Figure 6 for a low overpotential and for both cells. For the convective electrode, a slight variation with **B** appeared in the low-frequency domain of the capacitive loop. This behavior vanished by using the nonconvective electrode. Thus, the weak perturbation probably provoked by the MHD or natural convection in the low-frequency range was completely avoided by using a protected electrode. The flatness of the high-frequency semicircles observed for the low overpotentials did not lead to fitting with the experimental curves good accuracy by using eq 8. Nevertheless, the electrolytic current was kept constant versus **B**. Therefore, as the capacitive response did not change with **B**, the product $R_{ct}I$ was also assumed to be constant. This result confirmed the work described above, which has demonstrated that **B** did not influence the kinetic properties of the electrochemical process.

TABLE 1: C_d, R_{ct}, I, and $R_{ct}I$ Values for Different B Intensities[a]

	B/$T = 0$	**B**/$T = 0.15$	**B**/$T = 0.3$	**B**/$T = 0.45$	**B**/$T = 0.6$	**B**/$T = 0.75$	**B**/$T = 0.9$
$C_d/(\mu F \cdot cm^{-2})$	130	90	80	80	116	84	70
R_{ct}/Ω	28.4	12.6	10.8	9.1	8.7	8.7	8.0
I/mA	0.85	1.99	2.49	2.93	3.04	3.22	3.32
$R_{ct}I$/mV	24	25	27	27	26	28	27

[a] For experimental conditions, see Figure 4.

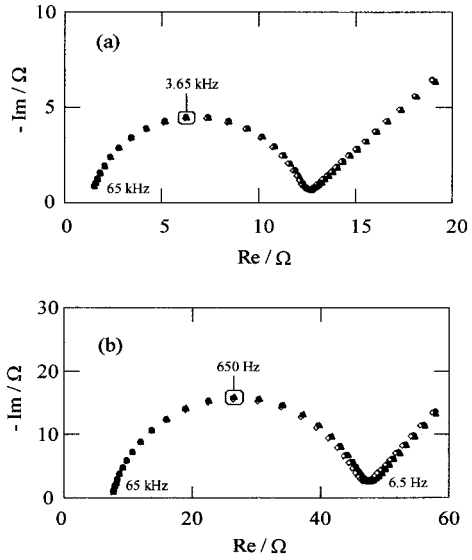

Figure 5. Electrochemical impedances in the Nyquist plane for various **B** intensities: (a) convective electrode, overpotential −17 mV, (b) nonconvective electrode, overpotential −43 mV; (●) **B** = 0, (◇) **B** = 0.3 T, (▲) **B** = 0.6 T. Fe(III)/Fe(II) redox system. [$FeCl_2$] = [$FeCl_3$] = 0.1 M, [HCl] = 4 M, electrode diameter 5 mm.

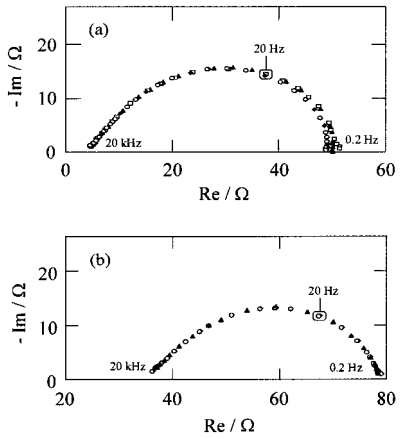

Figure 6. Electrochemical impedances in the Nyquist plane for various **B** intensities: (a) convective electrode, overpotential 15 mV, (b) nonconvective electrode, overpotential 17 mV; (○) **B** = 0, (◆) **B** = 0.45 T, (□) **B** = 0.6 T, (▲) **B** = 0.75 T. Cu^{2+}/Cu redox system. [$CuSO_4$] = 0.5 M, [H_2SO_4] = 0.5 M, electrode diameter 6 mm.

3. Kinetically Controlled Systems. *3.1. Nickel Electrodeposition from a Watts Bath*. The nickel electrodeposition from a pure Watts solution is known to be not limited by the mass transport process. Previous papers have highlighted **B** effects on the adsorption processes and on the structure of the deposit with a classical convective electrode.[22,23] It was demonstrated that the forced convection generated by **B** increased the diffusion flux of inhibiting species such as H^+ in a pure Watts bath. During nickel electrodeposition, the proton reduction on the working electrode induced an increase of the interfacial pH value, which led to changes in the adsorption kinetics, the texture, and the morphology of the electrodeposits. Thus, the influence of **B** in the low-frequency part of the impedance diagrams characteristic of the adsorption processes has already been studied in a previous paper.[23] Figure 7 shows the high-frequency responses obtained for different **B** intensities. For the convective electrode, the surface of the nickel working electrode was positioned downward. Concerning the nonconvective electrode, a vitreous carbon working electrode was facing upward. For both cells, the counter electrode was a large surface nickel electrode and the reference electrode was a SCE. The Watts solution was a mixture of $NiSO_4 \cdot 7H_2O$ (300 g/L), $NiCl_2 \cdot 6H_2O$ (35 g/L), and H_3BO_3 (40 g/L) at pH 4.5. Before each experiment, a nickel predeposit was carried out. For the convective electrode, a very slight shift of the impedance magnitude was observed when **B** was superimposed. In the presence of a protected electrode, this phenomenon completely disappeared. Once more, the modification generated by **B** on the transient response with a convective electrode was only due to a weak effect of the MHD convection induced at the electrode surface. The electrolytic current was kept practically constant for both cells as well as the fitted value R_{ct} obtained from eq 8. For the convective electrode and the nonconvective electrode, the product $R_{ct}I$ = 50 and 52 mV, respectively, for various magnetic inductions. Therefore, for a kinetically controlled system, the magnetic field did not affect the charge-transfer coefficient in the present experimental conditions. The C_d value was also practically constant versus **B**; $C_d = 90\ \mu F \cdot cm^{-2}$ for the convective electrode and $C_d = 80\ \mu F \cdot cm^{-2}$ for the nonconvective one.

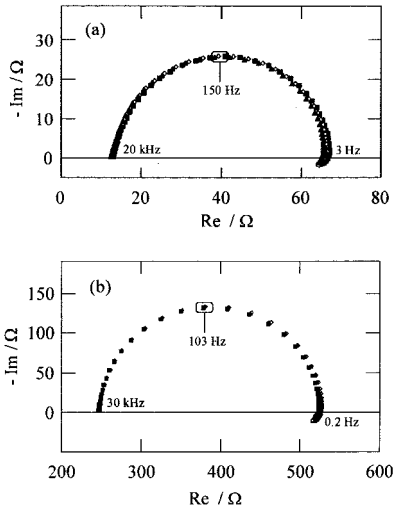

Figure 7. Electrochemical impedances in the Nyquist plane for various **B** intensities: (a) convective electrode, potential −840 mV/SCE, electrode diameter 6 mm, (b) nonconvective electrode, potential −860 mV/SCE, electrode diameter 3 mm; (■) **B** = 0, (◇) **B** = 0.3 T, (▲) **B** = 0.6 T. Nickel electrodeposition from a Watts bath.

3.2. Iron Dissolution in Acidic Media. The working electrode was an iron disk facing upward. The counter electrode was a large platinum sheet, and the reference electrode was a SSE. The electrolytic solution was a 1 M H_2SO_4 solution. The charge-transfer loops are given in Figure 8 for various **B** intensities. For both cells, a slight dispersion of the impedance modulus

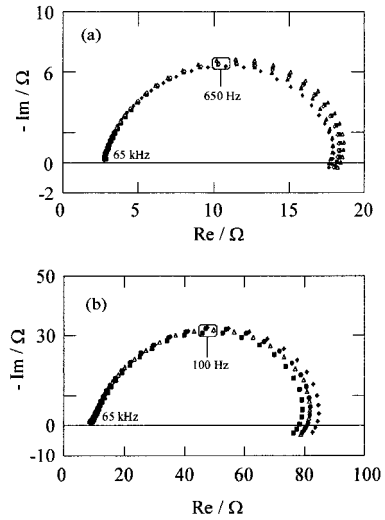

Figure 8. Electrochemical impedances in the Nyquist plane for various **B** intensities: (a) convective electrode, potential −880 mV/SSE, (◆) **B** = 0, (◇) **B** = 0.15 T, (▲) **B** = 0.3 T, (△) **B** = 0.45 T, (■) **B** = 0.6 T; (b) nonconvective electrode, potential −900 mV/SSE, (◆) **B** = 0, (△) **B** = 0.45 T, (■) **B** = 0.6 T, (●) = 0.75 T. Iron electrodissolution. $[H_2SO_4]$ = 1 M, electrode diameter 5 mm.

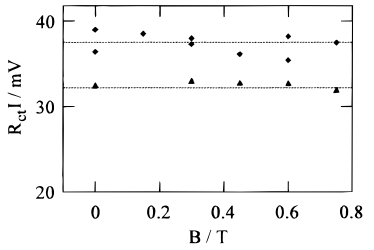

Figure 9. $R_{ct}I$ values versus **B**: (◆) convective electrode, (◆) nonconvective electrode. Experimental conditions the same as for Figure 8.

appeared in the presence of **B**. A dispersion of the current measurement was also noticed. This phenomenon was ascribed to the inaccurate reproducibility of the active surface during iron dissolution. For different **B** inductions, the R_{ct} value was fitted by means of eq 8. Figure 9 represents the product $R_{ct}I$ versus **B** for the convective electrode and the nonconvective one. Despite the dispersion in the R_{ct} and I values, the product $R_{ct}I$ was a constant for **B** intensities varying up to 1 T. Once more, this result demonstrated that **B** did not influence the charge-transfer kinetics process. It was also noticed that **B** did not modify the C_d value; $C_d = 330\ \mu F \cdot cm^{-2}$ for the convective electrode and $C_d = 265\ \mu F \cdot cm^{-2}$ for the nonconvective electrode.

Conclusion

From the EIS investigation of different electrochemical systems, mass transport controlled, kinetically controlled, and mixed electrochemical systems, we have shown that a homogeneous magnetic field up to 1 T parallel to the electrode surface does not practically modify the charge-transfer parameters of the process. This result was validated for different positions of the active surface of the working electrode, facing downward or upward or settled vertically. The weak effects observed in the presence of **B** were only due to a change of the electrode area during the metallic electrodeposition or electrodissolution, or due to the effect of the MHD convection. The latter effect was avoided by using a nonconvective electrode. Moreover, for the electrochemical systems studied in this paper and owing to the geometrical configuration of the system, the magnetic properties of the materials did not affect the experimental data, which concern the electrochemical kinetics.

References and Notes

(1) Fahidy, T. Z. *J. Appl. Electrochem.* **1983**, *13*, 553.

(2) Tacken, R. A.; Janssen, L. J. J. *J. Appl. Electrochem.* **1995**, *25*, 1.

(3) Lee, J.; Ragsdale, S. R.; Gao, X.; White, H. S. *J. Electroanal. Chem.* **1997**, *422*, 169.

(4) Leventis, N.; Chen, M.; Gao, X.; Canalas, M.; Zhang, P. *J. Phys. Chem. B* **1998**, *102*, 3512.

(5) Aogaki, R.; Fueki, K.; Mukaibo, T. *Denki Kagaku* **1975**, *43*, 509.

(6) Aaboubi, O.; Chopart, J. P.; Douglade, J.; Olivier, A.; Gabrielli, C.; Tribollet, B. *J. Electrochem. Soc.* **1990**, *137*, 1796.

(7) Devos, O.; Aaboubi, O.; Chopart, J. P.; Merienne, E.; Olivier, A.; Gabrielli, C.; Tribollet, B. *Pol. J. Chem.* **1997**, *71*, 1160.

(8) Chopart, J. P.; Devos, O.; Aaboubi, O.; Merienne, E.; Olivier, A. *Fluid Mechanics and its Applications*; Kluwer Academic Publishers: Dordrecht, The Netherlands, 1999; Vol. 51, p 181.

(9) Ragsdale, S. R.; Grant, K. M.; White, H. S. *J. Am. Chem. Soc.* **1998**, *120*, 13461.

(10) Grant, K. M.; Hemmert, J. W.; White, H. S. *Electrochem. Commun.* **1999**, *1*, 319.

(11) O'Brien, R. N.; Santhanam, K. S. V. *J. Appl. Electrochem.* **1997**, *27*, 573.

(12) Waskaas, M.; Kharkats, Y. I. *J. Phys. Chem. B* **1999**, *103*, 4876.

(13) Chopart, J. P.; Douglade, J.; Fricoteaux, P.; Olivier, A. *Electrochim. Acta* **1991**, *36*, 459.

(14) Fricoteaux, P.; Olivier, A.; Delmas, R. *J. Electrochem. Soc.* **1992**, *139*, 1096.

(15) Chiba, A.; Ogawa, T.; Yamshita, T. *Surf. Coat. Technol.* **1988**, *34*, 455.

(16) Danyliuk, A. L.; Kurmashen, V. I.; Matyushkov, A. L. *Thin Solid Films* **1990**, *189*, 247.

(17) Noninski, V. C. *Electrochim. Acta* **1997**, *42*, 251.

(18) Bard, A. J. *Anal. Chem.* **1961**, *33*, 11.

(19) Mark, H. B. *Anal. Chem.* **1964**, *36*, 958.

(20) Olivier, A.; Chopart, J. P.; Douglade, J.; Gabrielli, C. *J. Electroanal. Chem.* **1987**, *217*, 443.

(21) Devos, O.; Aaboubi, O.; Chopart, J. P.; Merienne, E.; Olivier, A.; Gabrielli, C.; Tribollet, B. *J. Phys. Chem. B* **1999**, *103*, 496.

(22) Devos, O.; Olivier, A.; Chopart, J. P.; Aaboubi, O.; Maurin, G. *J. Electrochem. Soc.* **1998**, *145*, 401.

(23) Devos, O.; Aaboubi, O.; Chopart, J. P.; Merienne E.; Olivier, A.; Amblard, J. *J. Electrochem. Soc.* **1998**, *145*, 4135.